ELSEVIER

Catalysis Today 70 (2001) 301–310

CATALYSIS TODAY

www.elsevier.com/locate/cattod

Dynamics of catalytic reactions on microdesigned surfaces

S.Y. Shvartsman [a,b], E. Schütz [c], R. Imbihl [c], I.G. Kevrekidis [b,*]

[a] *Department of Chemical Engineering, Massachusets Institute of Technology (MIT), Cambridge, MA 02139, USA*
[b] *Department of Chemical Engineering, Princeton University, Princeton, NJ 08544, USA*
[c] *Institut für Physikalische Chemie und Elektrochemie, Universität Hannover, Callinstr. 3-3a, D-30167 Hannover, Germany*

Abstract

We report experimental and computational studies of reaction dynamics on Pt/Rh and Pt/TiO_2 microcomposite catalytic surfaces. Reaction fronts initiated at the material interface dominate both steady and dynamic behavior of the composite catalytic material. Our analysis links the transient phenomenon of front initiation to the bifurcations of reaction–diffusion systems with active boundaries. © 2001 Published by Elsevier Science B.V.

PACS: 82.65.J; 05.45; 82.40.C

Keywords: Composite catalysts; Reaction dynamics; Fronts; Stability

1. Introduction

Controlling the spatiotemporal course of chemical reactions is an active area of research that spans many branches of science and engineering from cell biology to industrial reactor design. The problem can be approached through the engineering of well-defined reactor structures that would sustain a particular reaction regime. Recently, microlithography has been used to design catalytic reactors of various sizes, ranging from nano- to millimeters [1–4]. The spatial scale of lithographically fabricated reactors discussed in the current study is in the range of tens of microns. Building inert (TiO_2) walls around areas of Pt and Rh catalyst allowed us to isolate chemical reaction fronts, wavetrains and spirals [3,5–7]. An extension of this work, analyzing microdesigned catalysts with *several* active components [8,9], is presented in this paper. Using catalytic reduction of nitric oxide on composite (Pt/Rh) surfaces as our example, we illustrate how variations in composite size, geometry and boundary conditions can influence intrinsic nonlinear dynamics of catalytic reaction–diffusion systems. As in our previous studies, the size and the shape of a catalytic microreactor is manipulated with lithography, while boundary conditions are "implemented" by placing several active components with different reactivities next to each other. Here, we focus on critical effects, such as ignition and front propagation, mediated and affected by the presence of active boundaries.

The paper is organized as follows. In the next section we provide a brief description of the experimental set-up used in the study of microdesigned Pt/Rh composites. After that, we use mechanistic models of the NO reduction on Pt(1 0 0) and Rh(1 1 1) surfaces to show that, under reaction conditions used in this study, individual components of the composite catalyst can lie on the opposite branches of kinetic hysteresis. This motivates our phenomenological modeling and computational analysis of the steady state multiplic-

* Corresponding author. Tel.: +1-609-258-2818; fax: +1-609-258-0211.
E-mail address: yannis@princeton.edu (I.G. Kevrekidis).

0920-5861/01/$ – see front matter © 2001 Published by Elsevier Science B.V.
PII: S0920-5861(01)00338-8

ity patterns in a composite reaction–diffusion medium. Finally, we show that the basic phenomenology predicted by these models is observed in the experimental study of NO reduction on microdesigned catalysts. We conclude with an outline of some future directions for modeling and experimental studies of composite catalysts.

2. Experiments

The basic fabrication steps leading to the two-dimensional catalytic microstructures are shown in Fig. 1(left). A Pt single crystal of (1 0 0) orientation was covered with a polymer photoresist that was then lithographically developed in a negative photoresist process. Brief etching of the decorated surface in O_2 plasma, evaporation of Rh and lifting-off the remaining photoresist yielded a two-dimensional composite catalyst in which areas of bare Pt were surrounded by areas covered by, roughly, a 300 Å-thick polycrystalline layer of Rh (Fig. 1, right). The lateral intermixing of the two metals as determined with spatially resolved X-ray photoelectron microscopy (PEM) (or scanning photoelectron microscopy, SPEM) was shown to be restricted to an area of less than 2 microns. Reaction dynamics (at $T \approx 400$–500 K and pressures $<10^{-3}$ mbar) was observed by the photoemission electron microscopy (PEEM) [10]. The experiments were conducted in a standard UHV chamber operated as a gradient-free flow reactor under reaction conditions.

PEEM provides images of the local work function with lateral resolution of $\approx 1\,\mu$m and the time resolution of video frames (40 ms). The contrast in PEEM images mainly reflects the differences in the oxygen coverage [10]. The sharp contrast of the generated images stems from the fact that, under reaction conditions reported in this paper, the catalyst can be either in the oxygen-rich (dark, high work function) or in the oxygen-lean (bright, low work function) state.

3. Steady state multiplicity in catalytic NO reduction

Kinetic models of reactions on surfaces of individual components (Pt(1 0 0) and Rh(1 1 1)) account for the six experimentally identified surface species (NO, N, O, H, NH_x, NH_3) [11–14]. In the absence of kinetic data on the catalytic activity of thin (100–300 Å) Rh overlayers, we have modeled the Rh-covered part of the composite using the models (species, chemical reaction steps, rate constants) available for Rh(1 1 1) surface [11,12]. The models incorporate 12 surface reactions (the $NH_{2,ads}$ to $NH_{3,ads}$ and the OH_{ads} to H_2O steps are assumed instantaneous), see [15] for modeling details:

$$\text{(R1)}\ \mathrm{NO} + * \rightarrow \mathrm{NO_{ads}}, \quad \text{(R2)}\ \mathrm{NO_{ads}} \rightarrow \mathrm{NO} + *,$$

$$\text{(R3)}\ \mathrm{H_2} + 2* \rightarrow 2\mathrm{H_{ads}}, \quad \text{(R4)}\ 2\mathrm{H_{ads}} \rightarrow \mathrm{H_2} + 2*$$

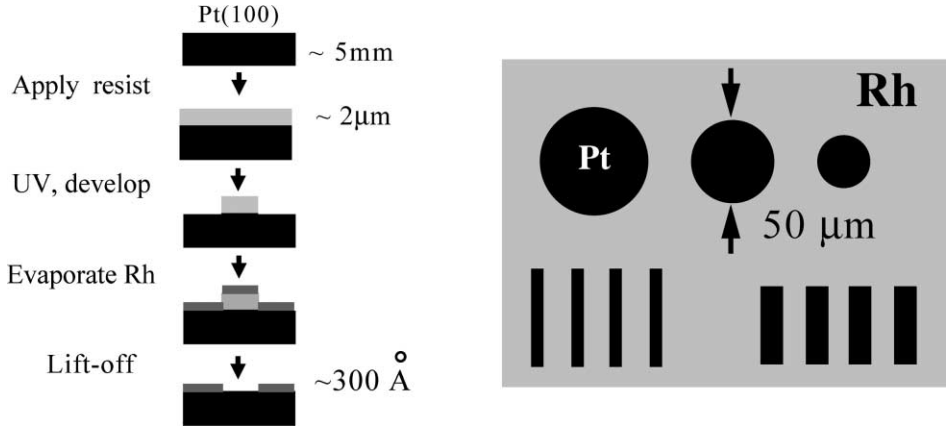

Fig. 1. Steps of the fabrication procedure (left) leading to a two-dimensional microcomposite catalyst (right).

(R5) $2N_{ads} \rightarrow N_2 + 2*$

(R6) $NO_{ads} + * \rightarrow N_{ads} + O_{ads}$,

(R7) $N_{ads} + O_{ads} \rightarrow NO_{ads} + *$,

(R8) $O_{ads} + H_{ads} \rightarrow OH_{ads} + *$

(R9) $N_{ads} + H_{ads} \rightarrow NH_{ads} + *$,

(R10) $NH_{ads} + * \rightarrow N_{ads} + H_{ads}$,

(R11) $NH_{ads} + H_{ads} \rightarrow NH_{2,ads}$,

(R12) $NH_{3,ads} \rightarrow * + NH_3$

The chemical basis of the steady state multiplicity in catalytic NO reduction becomes apparent after examining the key steps of the reaction mechanism. Both Pt(1 0 0) and Rh(1 1 1) readily chemisorb NO. Following that, the chemisorbed nitrosyl (NO_{ads}) dissociates into atomic adspecies (R6). While two nitrogen atoms quickly recombine and irreversibly desorb in the form of molecular nitrogen (R5), atomic oxygen stays on the surface below 800 K. Hence, a second reactant (H_{ads}) is required to remove it in the form of water (R8). (When the reducing agent is CO, the chemisorbed oxygen is removed from the surface in the form of CO_2.) On Pt(1 0 0) and Rh(1 1 1) surfaces, reactions (R5) and (R8) are much faster than (R1), which becomes the rate-limiting step. The first reaction in the pathway requires an empty surface site to proceed. However, the overall process generates an excess of empty sites upon completion, which provides an autocatalytic step in the overall reaction mechanism. The balance between the autocatalytic generation of the empty sites and their removal due to the chemisorption from the gas phase can be satisfied by three different compositions of the surface; this generates isothermal steady state multiplicity.

The Pt(1 0 0) surface binds hydrogen much stronger than Rh(1 1 1). Since the hydrogen species (H_{ads}) is crucial for the removal of the chemisorbed oxygen (O_{ads}), higher coverage by H_{ads} translates into higher catalytic activity. Rh(1 1 1), on the other hand, has a higher binding energy for oxygen, which leads to a lower surface coverage by H_{ads}. Due to these differences, individual metals (Pt and Rh, or Rh-covered Pt) will "ignite" and "extinguish" at different values of the operating parameters (p_{NO}, p_{H_2}, T).

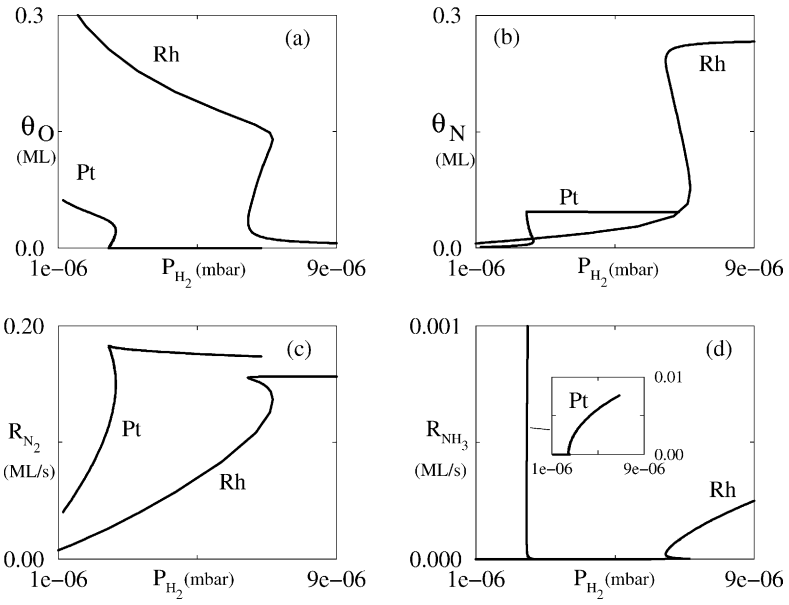

Fig. 2. Steady state multiplicity in the NO/H_2 reaction; $T = 470$ K, $P_{NO} = 2 \times 10^{-6}$ mbar. Results of a one-parameter continuation showing the dependence of surface coverages and reaction rates on the partial pressure of hydrogen, P_{H_2}. (a, b) Surface coverages of oxygen O_{ads} and nitrogen N_{ads}; (c, d) rates of nitrogen and ammonia production R_{N_2} and R_{NH_3}. The inset in (d) shows the rate of ammonia generation by a Pt(1 0 0) surface.

The pattern of isothermal steady state multiplicity computed for the surfaces of Pt and Rh as a function of P_{H_2} is presented in Fig. 2. On both the surfaces, the initial smooth decrease of oxygen coverage is followed by a transition to the state with very low oxygen coverage. It is precisely the abruptness of this transition that accounts for the sharp contrast in the PEEM images. The main conclusion arising from this one-parameter continuation is that for both metals, the transition between states of the surface with different reactivities ("dark/bright" transition) is through a saddle node bifurcation. Furthermore, in a wide range of parameters, surfaces of pure components can lie on different branches of the kinetic hysteresis. In the next section, we illustrate how surface diffusion couples with steady state multiplicity, mediating the spatially *nonuniform* transitions between different states of the surface.

4. Phenomenological modeling

We consider an idealized composite medium consisting of two components, A and B, arranged either in the form of alternating stripes (Fig. 3(a)) or circular inclusions (Fig. 3(b) and (c)). From now on, the domains will be called "domain A" and "domain B".

For a striped medium, with stripe lengths L_A and L_B, respectively, the model equations take the following form:

$$x \in (0, L_A): \quad u_t^A = D^A u_{xx}^A + F(u^A, \alpha_A, \lambda),$$

$$x \in (L_A, L_A + L_B): \quad u_t^B = D^B u_{xx}^B + F(u^B, \alpha_B, \lambda)$$

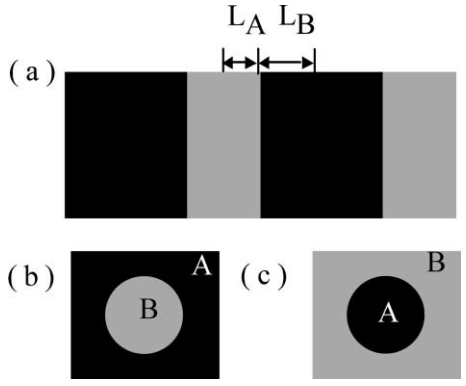

Fig. 3. Model composite medium: stripes (a) and circular inclusions (b, c).

$$u_x^B|_{L_B+L_A} = 0, \quad u_x^A|_0 = 0,$$

$$D^A u_x^A|_{L_A} = D^B u_x^B|_{L_A}, \quad u^A|_{L_A} = u^B|_{L_A}$$

With a cubic expression for the kinetic term, $F(u, \alpha, \lambda) = u - u^3 + \alpha + \lambda$, the dependence of the stationary solutions $u_s(\lambda)$ of $F(u_s(\lambda), \lambda)$ on λ (for constant α) will be hysteretic; see the characteristic S-shaped curves in Fig. 4(a)). To simulate two different materials, we choose $\alpha_A \neq \alpha_B$; this makes the boundaries of the hysteresis (with respect to λ) different for "materials" A and B. In this model, λ is the analog of the partial pressure of hydrogen in Fig. 2, whereas differences in α correspond to chemical differences between the Pt and the Rh parts of a composite surface. We call the upper and lower branches of this hysteresis "ignited" and "extinguished", respectively.

In the absence of diffusive coupling between the domains, the turning points, λ_E^A, λ_E^B ("E" for extinction) and λ_I^A, λ_I^B ("I" for ignition), of these S-shaped curves mediate *uniform* in space transitions between the solutions belonging to ignited and extinguished branches. Diffusive coupling of the adjacent domains leads to different types of nonuniform solutions, see Fig. 4(c). The turning points λ_E^U, λ_I^U are inherited from the bifurcation diagrams of individual materials. They mediate transitions from the almost uniform branches of steady states (U_E and U_I), whose solution in both of the domains is close to the everywhere extinguished/ignited states of the corresponding lumped problem. Notice, however, that there are two new turning points (λ_I^N and λ_E^N), bounding the region of existence of a branch of nonuniform solutions (denoted by "N" in the diagram) where only part of the domain is ignited. These nonuniform solutions exist only above certain critical length, note the cusp in Fig. 4(b).

Each of the four turning points seems to have a well-defined asymptote at large values of the domain size. The turning points that mediate the transitions from the uniform solutions asymptote to the corresponding values of the pure components. At the same time, the asymptotic value of λ_I^N (λ_E^N) coincides with the value of λ corresponding to the stationary front that exists in an infinite medium with kinetics of domain B (A). In a uniform medium, these fronts mediate transitions between the coexisting steady states. The fronts are stationary for a value of $\lambda = \lambda_{Max}$, for which the

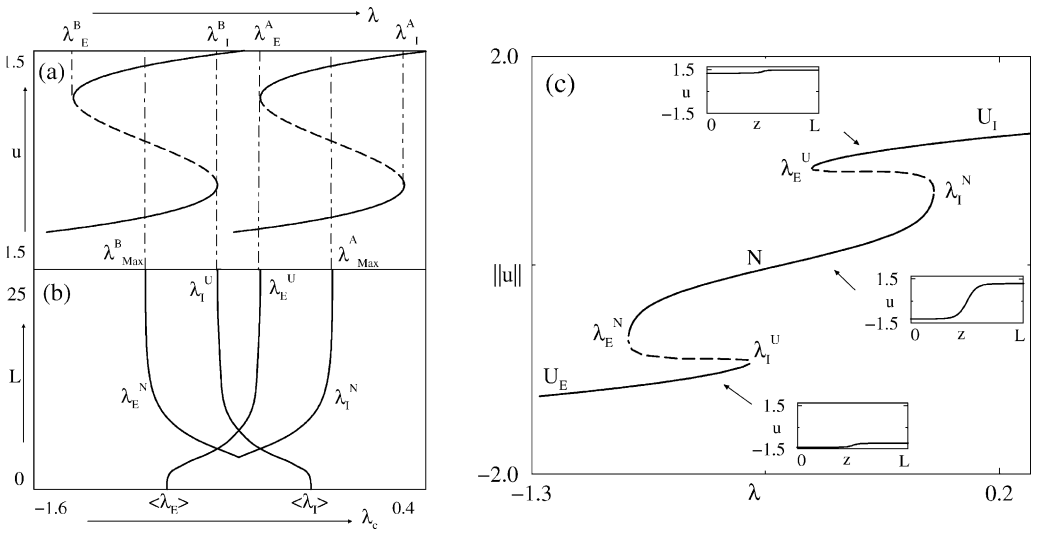

Fig. 4. Bistability in a model composite medium. (a) Kinetic hysteresis for individual components; (b) size dependence of the limit points in a "50/50" composite; (c) branch of steady states computed for $L = L_A + L_B = 15$; $D^A = D^B = 1$, $\alpha_A = 0$, $\alpha_B = 1$. The average over the domain is chosen as the solution norm, $\|u\|$. The two-parameter bifurcation diagram is symmetric, since the two domains have equal length ($L_A = L_B$). While this symmetry is destroyed for $L_A \neq L_B$, the large length asymptotes of each of the turning points are robust.

Maxwell condition holds: $\int_{u_-(\lambda)}^{u_+(\lambda)} F(u, \lambda, \alpha)\, du = 0$; $u_-(\lambda)$ and $u_+(\lambda)$ are extinguished and ignited steady states of the local kinetics [16].

Results of a one-parameter continuation, at large size of domain A, show that there exists a practically "vertical" branch of steady states, Fig. 5. Stationary solutions on the vertical part of the branch look (on domain A) like the stationary front, existing in an infinite A-medium at that parameter value, translated in a way that covers more and more of A with an ignited state. Indeed, the computed profiles in domain A (Fig. 5, inset) look like the fragments of a hyperbolic tangent (heteroclinic orbit for a cubic nonlinearity) translated to the left. As we move up the branch, the solution in which only domain B is ignited smoothly changes into one in which both of the domains belong to the ignited branch; this connection is clearly through the stationary realizations of the fronts in the infinite medium A. The intimate connection of these steady states with the self-similar A-medium solutions correlates with their practically neutral stability (leading eigenvalue of the linearization $\sim 10^{-4}$). The same type of behavior is observed in a transient simulation ensuing after a step-change in the parameter from $\lambda_1 < \lambda_{Max}$ to $\lambda_2 > \lambda_{Max}$, see Fig. 5(c).

We can simplify the analysis by converting the problem in two coupled domains into the problem in a single domain with appropriate boundary condition. We focus on the parameter regime where the domain B is

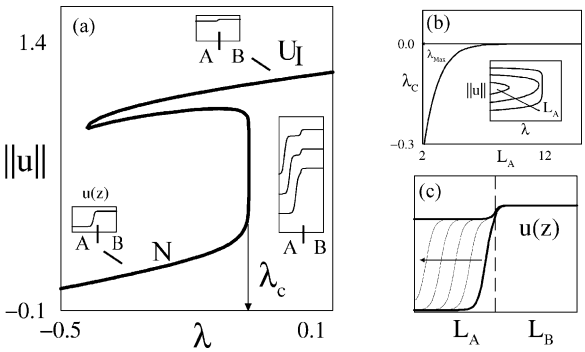

Fig. 5. Large length asymptote of turning points (boundaries of existence) of the nonuniform solution branch. (a) One-parameter bifurcation diagram computed for $L_A = L_B = 15$. Insets correspond to profiles of the uniformly extinguished and ignited solutions (lower and upper, respectively) and those on the "vertical" part of the diagram. (b) Asymptotic behavior of λ_I^N. The inset demonstrates the progressive "flattening" of the part of the diagram close to the instability. (c) Transient from a partially to a fully ignited state mediated by front propagation (see text for the details).

already ignited. The boundary condition is derived by first linearizing the PDE in domain B around the ignited steady state, $u_+^B(\lambda)$. Solving the resulting PDE to match the conditions at the material interface, we arrive at the following expression for the flux at the boundary of domain A:

$$D^A u_x^A = \kappa D^B \frac{u_+^B(\lambda) - u^A}{\delta(\lambda)}$$

where $\delta(\lambda) = \sqrt{-D^B/(\partial F^B(u_+^B(\lambda))/\partial u)}$. The factor κ depends on the curvature of the material interface (the interface is flat, convex and concave for the cases in Fig. 3(a), (b) and (c), respectively):

$$\kappa = 1 \qquad \text{flat interface}$$

$$\kappa = \frac{I_1(R/\delta(\lambda))}{I_0(R/\delta(\lambda))} < 1 \qquad \text{concave interface}$$

$$\kappa = \frac{K_1(R/\delta(\lambda))}{K_0(R/\delta(\lambda))} > 1 \qquad \text{convex interface}$$

where are $I_{0,1}$ and $K_{0,1}$ are modified Bessel functions for the first and second kind of orders 0 and 1.

The fact that $\kappa \neq 1$ in the case of the curved circular interfaces has an important effect on the shape of bifurcation diagram. The "almost" translational invariance present in the striped medium, which resulted in the vertical fragment of the branch, is now gone. There, the steady states on the vertical part of the diagram were related to stationary fronts. While the translation of a flat propagating interface does not affect its speed, motion of the axially symmetric front changes its curvature and as a result, leads to nonzero front acceleration [16]. In the case of a circular interface between domains, this inevitably leads to changes in the curvature of the incipient front and leads to the "bending" of the vertical fragment in the bifurcation diagram.

Fig. 6 illustrates the radial dependence of the solution for the case of a circular inclusion surrounded by a "sea" of material B. As before, the solution loses stability to a fully ignited state at a critical value of parameter λ_c. The transversality condition required for the saddle-node bifurcation is satisfied in this case, and the branch turns backward after the point of instability. Contour plots of the radially symmetric stationary solutions at different points along the branch are shown in Fig. 6(d); they appear as radially

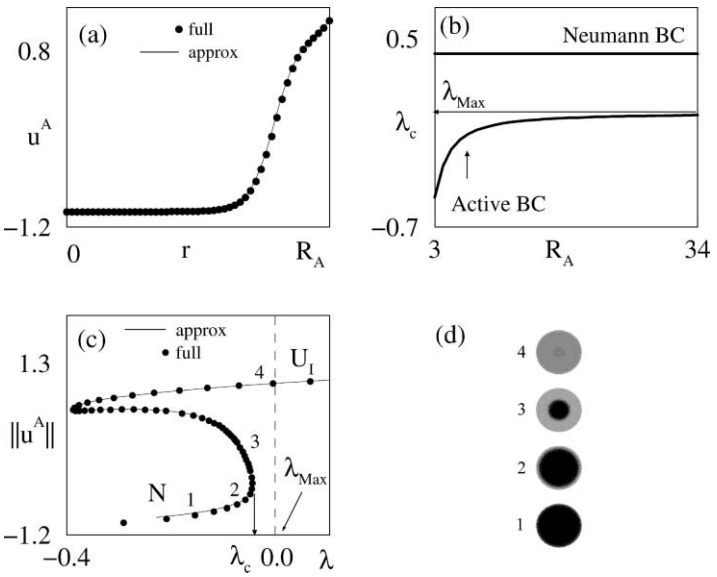

Fig. 6. Ignition from circular interfaces, Fig. 3(c). (a) Steady states computed with the full and the reduced BC formulations ($R_A = 15$, $\lambda = -0.2$); (b) two-parameter bifurcation diagram showing the ignition turning point dependence on the radius of domain A; (c) branch of steady states computed for $R_A = 15$; (d) gray scale plots showing the steady states corresponding to locations (1, 2 ,3, 4) in (c); black/gray corresponds to extinguished/ignited regions, respectively.

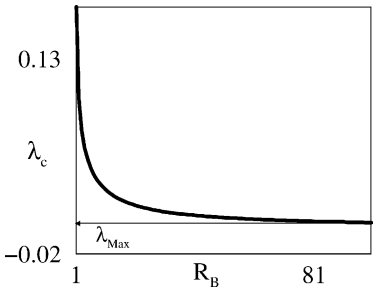

Fig. 7. "Outward" ignition from circular interfaces, Fig. 3(b). Two-parameter bifurcation diagram showing turning point dependence on the radius of ("igniting inclusion") domain B. Computations were performed with an annulus of material "A" with $R_A = 25$, Neumann boundary condition was imposed at R_A. Inset: part of the branch close to the saddle-node bifurcation.

symmetric fronts with an increasing fraction of the ignited region as we move up the nonuniform ("N") branch. This shift of λ_c to the left of λ_{Max} is expected to become less important for large radii of the domain A. The two-parameter bifurcation diagram presented in Fig. 6(b) shows that at large values of R_A, λ_c again asymptotes to the value predicted from the front stationarity condition (λ_{Max}).

The situation is exactly the opposite in the case of a circular inclusion sending an ignition front outwards, see Fig. 3(b). The curvature of the interface *decreases* as the front expands and most importantly is close to the boundary between the domains. Since an expanding front has a speed less than that of a flat counterpart, the location of the instability leading to the front inception happens beyond (in λ) the value dictated by the stationarity condition; the large radius limit, however, is again λ_{Max}, see Fig. 7.

5. Experimental observations

We present two experimental observations illustrating the effects of the boundaries on (i) transient dynamics, and (ii) bifurcation behavior of microreacting domains.

We first describe a *dynamic* effect due to the presence of an active boundary on a composite surface (i.e., of a neighboring domain of a different catalytic activity). Fig. 8 captures instances of a transient phenomenon ensuing on the composite surface after a step-change in operating conditions. A step-change in p_{H_2} from 2×10^{-6} to 7×10^{-6} mbar (at constant $p_{NO} = 2 \times 10^{-6}$ mbar and $T = 473$ K) leads to the development of a bright rim at the Pt/Rh interface and initiates a front propagating *outwards* from the boundary. The front, moving at a speed of $\sim$1 μm/s, leaves the Rh-covered surface in the reactive (PEEM bright) state. Time histories of local work function measurements made in the middle of Pt domain and at a point on the Rh-covered part of the surface (sufficiently far from the boundary) are qualitatively different, see Fig. 9(a). Following the step-change in p_{H_2} (Fig. 9(b)), the Pt, that was initially in the "PEEM-dark", unreactive state "A" in Fig. 9(c) undergoes a transient leading to a new "PEEM-bright" steady state ("E" in Fig. 9(c)) corresponding to the new partial pressure of hydrogen. A typical location on the Rh surface, on the other hand, first undergoes transition to an

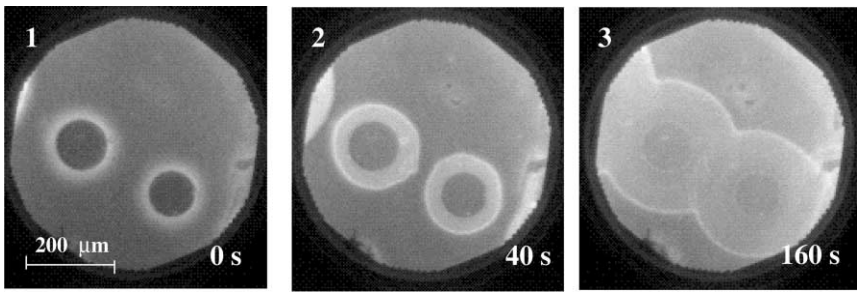

Fig. 8. PEEM images of the microstructured Pt(1 0 0)/Rh surface showing a transition from the unreactive/oxygen-covered state to the reactive/largely oxygen-free state in the $NO + H_2$ reaction. Reaction fronts nucleate at the perimeter of the dark circles (frame 1) which represent circular Pt(1 0 0) domains surrounded by Rh. The transition was initiated by a p_{H_2} increase from 2×10^{-6} to 7×10^{-6} mbar. Experimental conditions: $p_{NO} = 2 \times 10^{-6}$ mbar; $T = 473$ K.

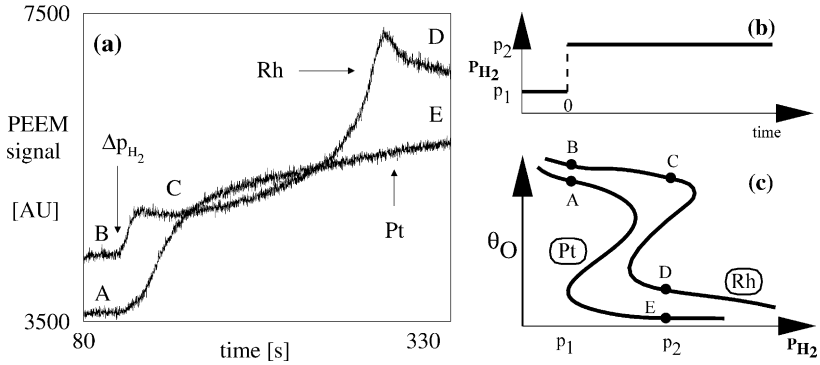

Fig. 9. (a) Time histories of PEEM signal measured at two different locations on the composite catalyst of Fig. 8: at the center of the Pt circle and on the Rh part of surface, at 100 μm from the material interface. (b), (c) Qualitative representation of the step-change in the partial pressure of hydrogen and the states of the surface (oxygen coverage, θ_O) at different stages of the spatiotemporal transient (see text for details).

intermediate (metastable) state ("C" in Fig. 9(c)) where it stays for some time and then jumps to the final, brighter, state ("D" in Fig. 9(c)). Different stages of the transient are interpreted as transitions between two stable steady states coexisting on the Rh-covered part of the surface at the new value of the p_{H_2}. The first transition is "uniform" in the sense that it is brought about by a uniform change of the operating parameter and happens almost simultaneously for all locations on the Rh-covered surface. The second transition, on the other hand, is mediated by the propagation of the reaction front and happens with a time delay determined by (and increasing with) the distance of a particular location on the Rh-covered surface from the Pt/Rh boundary.

Analysis of the phenomenological model predicted qualitative differences in the size dependence of bifurcation points for circular domains with inert boundaries versus those with active boundaries. Data in Fig. 10, presenting the bifurcation properties of circular Pt domains catalyzing the NO + CO reaction, demonstrate this effect experimentally. In the reaction $NO + CO \rightarrow \frac{1}{2}N_2 + CO_2$ at 300 K, the surface is in its inactive state, fully covered by molecular NO/CO adsorbate. The reactivity of the Pt(1 0 0) surface at low temperature is limited by the availability of vacant sites necessary for the dissociation of NO. Upon slow heating, however, a sharp transition ("surface explosion") to the reactive state occurs as the combined NO/CO coverage falls below 0.5, triggering an autocatalytic increase in the number of vacant sites. In the experiments the ignition temperature (T_{ign}) (at partial pressures $p_{NO} = 1.2 \times 10^{-5}$ mbar and $p_{CO} = 0.9 \times 10^{-5}$ mbar), corresponding to the transition from the unreactive to the reactive branch of the kinetic hysteresis was measured as a function of the radius of the Pt domains (R_{Pt}). While T_{ign} is essentially constant for domains surrounded by inert TiO_2, it becomes a function of R_{Pt} when the Pt

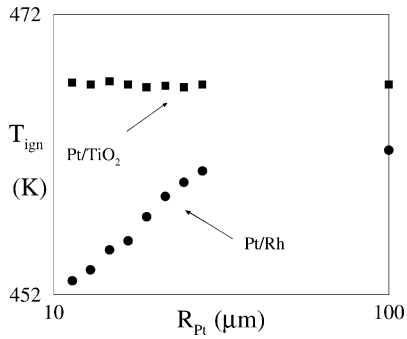

Fig. 10. Influence of the boundary conditions and the domain size on the ignition of a molecularly adsorbed NO/CO layer on Pt(1 0 0). The plot shows the dependence of the ignition temperature T_{ign} on the domain radius for circular Pt domains surrounded by a reactive 500 Å Rh layer (circles) or by an unreactive 500 Å Ti/TiO_2 layer (squares). The samples were slowly heated in a NO/CO atmosphere starting from 300 K. Experimental conditions: $p_{NO} = 1.2 \times 10^{-5}$ mbar, $p_{CO} = 0.9 \times 10^{-5}$ mbar; heating rate during ignition experiment 0.1 K/s.

circle is surrounded by more active Rh. The process of (isothermal) ignition is initiated at the boundary of the circle and *propagates inwards*. The observations may be interpreted chemically as an effective *inflow* of empty sites into the Pt domain through its boundary with the more active, Rh-covered part of the composite. The independence of T_{ign} on R_{Pt} in the case of inert boundaries can be rationalized in terms of a bifurcation diagram of a kinetically bistable system with Neumann boundary conditions.

6. Discussion

We have analyzed the spatiotemporal dynamics observed on Pt/Rh microcomposite catalytic surfaces in terms of diffusive coupling between distinct reactive domains. Our main focus was on critical effects, such as steady state multiplicity and front propagation. One of the contributions of this study is the analysis of the limiting behavior of turning points bounding the existence of the nonuniformly ignited solutions. In the case of the instability mediating the transition from partially to fully ignited states, we found that the exchange of stability is accompanied by a characteristic vertical fragment of the bifurcation diagram. The "almost neutral stability" of the steady states belonging to the vertical part of the branch, as well as the front-like nature of the transients following the step-changes of the parameter past the critical value, point to their close connection with the stationary fronts supported by the corresponding homogeneous medium. For the case of circular interfaces, we have shown that the vertical fragment of the branch "bends" to become a part of the regular saddle-node picture. Previous experimental work indicates that the early time dynamics of the transients associated with the "ignitions from the boundary" are strongly affected by the shape of the interface [17]. In the case of the scalar reaction diffusion systems, we were able to capture the effect of diffusive coupling between two components by Robin boundary conditions.

Several physico-chemical issues have to be addressed before employing the existing models of NO surface chemistry for the direct interpretation of data obtained with microdesigned catalysts. Most importantly, models for the interface between the individual catalytic components have to be developed, assuming the existence of a sharp material interface changes one of the boundary conditions in the composite reaction–diffusion problem. Specifically, instead of the continuity of value, the continuity of chemical potential has to be imposed. Using a Lagmuir description for a single-species adlayer in a model problem, we have shown that this boundary condition leads to solutions that are discontinuous across the material interface [18]. The main effects reported in this study however — the presence of the vertical branch in the bifurcation diagram, the fact that the stability boundary of the partially ignited state lies below the one corresponding to the uniform medium, and the fact that overstepping the new stability boundary results in the initiation of a propagating front — were found to be robust. Furthermore, the derivation of the effective boundary condition can be carried out without any difficulties. The nonlinearity of chemical potential translates into the nonlinearity in the effective boundary condition; this, however, poses no obstacles for the computational analysis. The next step in the modeling of catalytic composites must address alloying between different components. Preliminary experimental results obtained with spatially resolving XPS spectroscopy [19] indicate that alloying, especially prominent at the interface between materials, plays an important role in front initiation [8] and hence in the stability boundaries of different reacting regimes. A point relevant for the Pt/Rh system is that reactive and transport properties of the alloy at the component interface may differ from those anticipated by simple averaging of properties of pure components [20].

Lithographic design offers systematic ways of constructing controlled heterogeneities in catalytic materials. The ability to both isolate microreacting domains and couple them to media with different reactive properties enables the direct testing of rapidly developing theories of dynamics in microstructured materials and materials with localized perturbations [21–23]. Close coupling of experiments, theory and simulations in the analysis of catalytic composites is bound to generate new insights into the behavior of man-made and natural microreacting systems.

Acknowledgements

This work was partially supported by the National Science Foundation and the Alexander von Humboldt Foundation.

References

[1] K. Wong, S. Johansson, B. Kasemo, Nanofabricated model catalysts — manufacturing and model studies, Faraday Discuss. 105 (1996) 237–246.

[2] M.X. Yang, D.H. Gracias, P.W. Jacobs, G.A. Somorjai, Lithographic fabrication of model systems in heterogeneous catalysis and surface science studies, Langmuir 14 (6) (1998) 1458–1464.

[3] M.D. Graham, I.G. Kevrekidis, K. Asakura, J. Lauterbach, K. Krischer, H.H. Rotermund, G. Ertl, Effects of boundaries on pattern formation in catalytic oxidation of CO on platinum, Science 264 (5155) (1994) 80–82.

[4] R. Srinivasan, I.M. Hsing, P.E. Berger, K.F. Jensen, S.L. Firebaugh, M.A. Schmidt, M.P. Harold, J.J. Lerou, J.F. Ryley, Micromachined reactors for catalytic partial oxidation reactions, AIChE J. 43 (11) (1997) 3059–3069.

[5] G. Haas, M. Bär, I.G. Kevrekidis, P.B. Rasmussen, H.H. Rotermund, G. Ertl, Observation of front bifurcations in controlled geometries: from one to two-dimensions, Phys. Rev. Lett. 75 (19) (1995) 3560–3563.

[6] N. Hartmann, M. Bär, I.G. Kevrekidis, K. Krischer, R. Imbihl, Rotating chemical waves in small circular domains, Phys. Rev. Lett. 76 (18) (1996) 1384–1387.

[7] M.D. Graham, M. Bär, I.G. Kevrekidis, K. Asakura, J. Lauterbach, H.H. Rotermund, G. Ertl, Catalysis on microstructured surfaces — pattern formation during CO oxidation in complex Pt domains, Phys. Rev. E 52 (1) (1995) 76–93.

[8] E. Schütz, N. Hartmann, I.G. Kevrekidis, R. Imbihl, Catalysis on microstructured surfaces, Faraday Discuss. 105 (1996) 47–56.

[9] E. Schütz, N. Hartmann, I.G. Kevrekidis, R. Imbihl, Microchemical engineering of catalytic reactions, Catal. Lett. 54 (4) (1998) 181–186.

[10] H.H. Rotermund, Imaging of dynamic processes on surfaces by light, Surf. Sci. Rep. 29 (7) (1997) 267–364.

[11] A.G. Makeev, M.M. Slinko, N.M.H. Janssen, P.D. Cobden, B.E. Nieuwenhuys, Kinetic oscillations and hysteresis phenomena in the $NO+H_2$ reaction on Rh(1 1 1) and Rh(5 3 3): experiments and mathematical modeling, J. Chem. Phys. 105 (16) (1996) 7210–7222.

[12] A.G. Makeev, B.E. Nieuwenhuys, Mathematical modeling of the $NO+H_2$/Pt(100) reaction: surface explosion, kinetic oscillations, and chaos, J. Chem. Phys. 108 (9) (1998) 3740–3749.

[13] P.D. Cobden, N.M.H. Janssen, Y. van Breugel, B.E. Nieuwenhuys, Non-linear behaviour in the $NO+H_2$ reactions over single crystals and field emitters of some Pt-group metals, Faraday Discuss. 105 (1996) 57–72.

[14] M. Gruyters, A.T. Pasteur, D.A. King, Simulation of oscillatory behaviour in the reduction of NO by hydrogen on Pt(1 0 0): the role of non-linear restructuring, J. Chem. Soc. Farad. Trans. 92 (16) (1996) 2941–2949.

[15] S.Y. Shvartsman, Ph.D. Thesis, Princeton University, Princeton, NY, USA, 1999.

[16] A.S. Mikhailov, Foundations of Synergetics, Springer, Berlin, 1994.

[17] J. Lauterbach, H.H. Rotermund, P.B. Rasmussen, M. Bär, M.D. Graham, I.G. Kevrekidis, G. Ertl, Catalysis on mesoscopic composite surfaces: influence of palladium boundaries on pattern formation during CO oxidation on Pt(1 1 0), Physica D 123 (1998) 493–501.

[18] X. Li, S.Y. Shvartsman, R. Imbihl, I.G. Kevrekidis, Front initiation in structured reaction–diffusion systems, 2001, submitted to Chaos, 2001.

[19] F. Esch, S. Günther, E. Schütz, A. Schaak, I.G. Kevrekidis, M. Marsi, M. Kiskinova, R. Imbihl, Chemically resolved dynamical imaging of catalytic reactions on composite surfaces, Catal. Lett. 52 (7) (1998) 85–90.

[20] H. Hirano, T. Yamada, K.I. Tanaka, J. Siera, B.E. Nieuwenhuys, Z. Shay, R.W. Joyner, J.H. Block, R.A. van Santen, D. Chadwick, G.B. Fisher, G.A. Somorjai, The reduction of nitric oxide by hydrogen over Pt, Rh and Pt–Rh single crystal surfaces, Stud. Surf. Sci. Catal. 75 (1993) 345–357.

[21] S. Torquato, Random heterogeneous media: microstructure and improved bounds for effective properties, Appl. Mech. Rev. 44 (1991) 37–87.

[22] M.J. Ward, J.B. Keller, Nonlinear eigenvalue problems under strong localized perturbations, Stud. Appl. Math. 85 (1) (1991) 1–28.

[23] G.I. Barenblatt, J.B. Bell, W.Y. Crutchfield, The thermal explosion revisited, Proc. Nat. Acad. Sci. 95 (23) (1998) 13384–13386.